Journal Name

ARTICLE

High Performance Inverse Opal Li-ion Battery with Paired Intercalation and Conversion Mode Electrodes

Received 00th January 20xx,
Accepted 00th January 20xx

DOI: 10.1039/x0xx00000x

www.rsc.org/

David McNulty,[a] Hugh Geaney, [a] Eileen Armstrong, [a] and Colm O'Dwyer [a,b]*

Structured porous materials have provided several breakthroughs that have facilitated high rate capability, better capacity retention and material stability in Li-ion batteries. However, most advances have been limited to half cells or lithium batteries, and with a single mode of charge storage (intercalation, conversion, or alloying etc.). The use of dual-mode charge storage with non-traditional material pairings, while maintaining the numerous benefits of nanoscale materials, could significantly improve the capacity, energy density, stability and overall battery safety considerably. Here, we demonstrate an efficient, high capacity full inverse opal Li-ion battery with excellent cycle life, where both the cathode and anode binder-free electrodes are composed of 3D nanocrystal assemblies as inverse opal (IO) structures of intercalation-mode V_2O_5 IO cathodes and conversion-mode Co_3O_4 IO anodes. Electrochemically charged Co_3O_4 IOs function as Li-ion anodes and the full V_2O_5/Co_3O_4 cell exhibits superior performance compared to lithium batteries or half cells of either IO material, with voltage window compatibility for high capacity and energy density. Through asymmetric charge-discharge tests, the V_2O_5 IO/Co_3O_4 IO full Li-ion cell can be quickly charged, and discharged both quickly and slowly without any capacity decay. We demonstrate that issues due to the decomposition of the electrolyte with increased cycling can be overcome by complete electrolyte infiltration to remove capacity fading from long term cycling at high capacity and rate. Lastly, we show that the V_2O_5 IO/Co_3O_4 IO full Li-ion cells cycled in 2 and 3-electrode flooded cells maintain 150 mAh g^{-1} and remarkably, show no capacity fade at any stage during cycling for at least 175 cycles. The realization of an all-3D structured anode and cathode geometry with new mutually co-operative dual-mode charge storage mechanisms and efficient electrolyte penetration to the nanocrystalline network of material provides a testbed for advancing high rate, high capacity, stable Li-ion batteries using a wide range of materials pairings.

A Introduction

Li-ion batteries have become ubiquitous in everyday applications from cell phones to portable electronics. With increasingly challenging energy demands for these devices, the development of Li-ion batteries with increased specific energies and better cycle life is highly sought after. [1-3] Furthermore, the development of batteries that would allow the electrification of vehicular fleets is important and timely, with advanced Li-ion battery chemistries and 'beyond Li-ion' (e.g. Li-S, Li-O_2) as possible candidates. [4-7] With the practical energy densities achievable using beyond Li-ion systems still far from established (owing to demanding battery chemistries and increased instabilities compared to Li-ion systems), the development of advanced Li-ion batteries remain a topic of utmost importance.

A wide range of materials have been investigated for advanced Li-ion applications in terms of both the cathode and anode. The development of cathode materials with high specific capacities is a challenging task but significant progress has been made in the synthesis of different Li containing transition metal oxide compounds (containing some or all of Ni, Mn and Co) [8-12] and other compounds such as $LiFePO_4$ [13, 14] and V_2O_5 [15-17]. Similarly, a plethora of different anode materials have been investigated from classic intercalation materials (graphite and other forms of carbon) [18-21] to alloying materials (particularly Si, Sn and Ge) [22-25] and conversion materials such as NiO and Fe_2O_3. [26-28] Alloying and conversion materials offer potential for higher gravimetric capacities compared to conventional graphitic anodes due to differences in the lithium storage mechanisms beyond simple intercalation. [1, 29]

In addition to the identification of suitable electrode materials, a dedicated research effort has been made into the development of 3D or networked material architectures to optimize cycling performance. [30-33] In recent years, three-dimensional ordered macroporous (3DOM) materials such as inverse opals (IO)[34] have proven very useful for increase cycling stability. [35-37] The physical properties of IO structured materials have many potential benefits for use in Li-ion batteries.[38] The surface area for IO structures comparison 3D assemblies of nanocrystalline material is relatively large and

[a] Department of Chemistry, University College Cork, Cork, T12 YN60, Ireland.
[b] Micro-Nano Systems Centre, Tyndall National Institute, Lee Maltings, Cork, T12 R5CP, Ireland.
* E-mail: c.odwyer@ucc.ie; Fax: +353 (0)21 4274097; Tel: +353 (0)21 4902732
Electronic Supplementary Information (ESI) available: Additional information on the Co_3O_4 IO anode structure and electrochemistry, and supplementary figures. See DOI: 10.1039/x0xx00000x

the macropores allow a high surface area of the active material to be in direct contact with the electrolyte. [39] The thin walls surrounding the pores offer reduced Li^+ diffusion path lengths compared to larger scale materials and also the 3D networked nature of an IO structure can provide continuous transport paths and ensure good electronic and also ionic conductivity. [40] The bicontinuous IO electrode materials reported by Braun [41] and Stein [42] have demonstrated impressive capacity retention when tested as lithium batteries, or half-cell Li-ion anodes, and interdigitated forms of IO-type electrodes should allow a higher tap density of active material without negating the inherent benefits of the 3D structuring to enhancing the cell performance. The majority of reports detailing the development of novel anode and cathode systems for Li-ion batteries conduct electrochemical characterization of the materials vs a Li counter electrode. [43] While this is a useful means of determining performance in lab scale tests (and allows fundamental characterization of phase changes associated with operation and capacity retention with cycling etc.), the commercial use of Li in full cells has been largely avoided due to well established issues related to safety. [44-47] As a result of the unsuitability of bulk Li as an electrode material for practical systems; it is more useful to consider anode and cathode material pairings that possess compatible operating voltage windows. Reports on promising cathode and anode materials typically only focus on half-cell performance and surprisingly, reports on successful full Li-ion cells remain quite uncommon, yet improvement in stability, power and energy densities could be achieved when 3D structure materials are brought into close contact [48] and utilize pairs of materials that offer mutually beneficial charge storage modes, high cycle life, capacities and useful voltages.

When full Li-ion cells are reported either the cathode or anode material being investigated is typically cycled against the corresponding, most commonly used cathode or anode materials (often olivines, spinels or variants of LiM_xO_y, LiM_xPO_y (M = metal)) or graphite, respectively. We report the first all inverse opal Li-ion battery using binder-free V_2O_5 intercalation cathodes and Co_3O_4 conversion-mode anodes. We detail the structural and electrochemical nature of the pre-charged Co_3O_4 inverse opal networked material as a high capacity (>200 mAh g^{-1} after 100 cycles) Li-ion battery anode and through cyclic voltammetry and galvanostatic testing, demonstrated the V_2O_5/Co_3O_4 IO cell provides a stable, high capacity Li-ion cell that retains ~150 mAh g^{-1} over 175 cycles and excellent rate capability and capacity retention during symmetric and asymmetric (slow discharge, fast charge) conditions.

B Experimental

The Co_3O_4 IO was prepared by a two-step process. Firstly, a solution of polystyrene (PS) spheres (Polysciences Inc.) in isopropanol was drop cast on to 1 cm^2 pieces of stainless steel; the sphere templates were then infilled with a 0.1 M solution of $CoCl_2$ in IPA. The diameter of the PS spheres used was ~ 500 nm. Secondly, the infilled spheres where heated at 450 ^oC in air for 12 h, to remove the sphere templates and to crystallize the samples. V_2O_5 IO samples were prepared by a two-step process. Firstly, PS spheres were electrophoretically deposited on a stainless steel substrate. Secondly, the sphere template was infilled by electrodeposition of a vanadyl sulfate solution. The working electrode was consisted of a PS sphere template coated stainless steel substrate, the counter electrode was platinum mesh and the reference was a saturated calomel electrode (SCE). The electrolyte was a 0.25 M solution of vanadium (IV) oxide sulfate hydrate (Sigma Aldrich) in a 1:1 (v/v) mixture of ethanol and deionized water. The sphere template was infilled by applying a constant potential of 2.0 V (vs SCE) for 900 s. Samples were then heated to 300 ^oC in air for 12 h, to remove the sphere template.[49, 50] The mass loading for V_2O_5 and Co_3O_4 IO samples was ~ 1-2 mg.

TEM analysis was conducted using a JEOL JEM-2100 TEM operating at 200 kV. SEM analysis was performed using an FEI Quanta 650 FEG high resolution SEM at an accelerating voltage of 10 kV. XRD analysis was performed using a Phillips Xpert PW3719 diffractometer using Cu Kα radiation. (Cu Kα, λ = 0.15418 nm, operation voltage 40 kV, current 40 mA). All electrochemical results presented in this report were performed using a BioLogic VSP Potentiostat/Galvanostat. The electrolyte consisted of a 1 mol dm^{-3} solution of lithium hexafluorophosphate salts in a 1:1 (v/v) mixture of ethylene carbonate in dimethyl carbonate + 3 wt% vinylene carbonate. The electrochemical properties of Co_3O_4 IO and V_2O_5 IO materials were investigated in a half cell configuration against a pure Li counter electrode in a two electrode, stainless steel split cell (a coin cell assembly that can be disassembled for post-mortem analysis). No additional conductive additives or binders were added. For testing in a full cell arrangement against a V_2O_5 IO cathode, the Co_3O_4 IO anode was electrochemically pre-charged by a single charge against a Li metal counter electrode. The separator used in all split cell tests was a glass fiber separator (El-Cell ECC1-01-0012-A/L, 18 mm diameter, 0.65 mm thickness). Cyclic voltammetry for the V_2O_5 IO/Co_3O_4 IO full Li-ion cells was performed using a scan rate of 0.1 mV s^{-1} in a potential window of 3.0 – 0.2 V. Galvanostatic testing, rate capability and asymmetric testing were performed in 2 electrode split cells and also in 3-electrode flooded cells in a potential window of 3.0 – 0.2 V.

C Results and discussion

An SEM image of a typical V_2O_5 IO electrode prepared from vanadyl sulfate electrodeposition [49] into artificial opal templates, shown in Figure 1a, the thickness of the IO material on the stainless steel substrate was ~27.08 µm, as shown in Figure S1a. The walls of the IO structure are comprised of an agglomeration of nanoscale crystallites of vanadium oxide as can be seen in Figure S2. V_2O_5 IO electrodes were tested as a cathode material in a half cell configuration against a pure Li metal counter electrode. The discharge and charge voltage profiles for the second cycle are shown in Figure 1b. The specific capacity values obtained over 50 cycles are shown in Figure 1c. Initial capacities were ~ 150 mAh g^{-1}, which is

comparable to specific capacities reported for various cathode materials, including $LiCoO_2$ [51], $LiFePO_4$ [52], $LiMn_2O_4$ [53] and $Li(Ni_{1/3}Mn_{1/3}Co_{1/3})O_2$ [9]. The specific capacity after 50 cycles was ~89.35 mAh g^{-1}. Similar capacity values have been reported for other V_2O_5 nanostructured cathode materials. [54-58] Co_3O_4 IO were prepared by infilling of a polystyrene sphere template with a 0.1 M $CoCl_2$ solution on a stainless steel substrate and then annealing the samples to at 450 °C for 12 h. Co_3O_4 "macrobowls" have previously been reported [59], however to our knowledge the synthesis procedure contained herein represents the first report of a phase pure, nanocrystalline Co_3O_4 inverse opal structure, with a periodicity close to 500 nm of the parent opal template. Calcination of the infilled sphere template samples, resulted in an IO network with pore sizes < 500 nm, as shown in Figure 1d, and walls comprising assemblies of networked nanocrystals. The thickness of a typical Co_3O_4 IO material was determined to be ~29.70 µm as shown in Figure S1b. The XRD pattern for a Co_3O_4 IO, shown in Figure S3, was successfully indexed to pure fcc Co_3O_4 (JCPDS No. 42-1467).

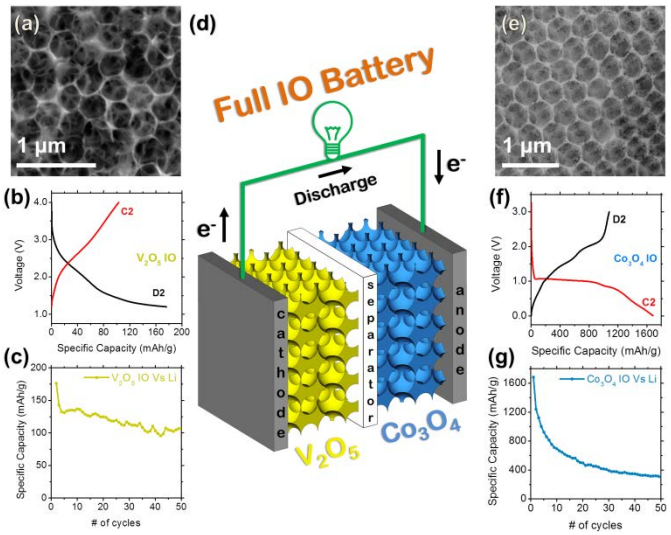

Fig. 1. The behaviour of individual V_2O_5 IO cathodes and Co_3O_4 IO anodes in lithium half cells. (a) SEM image, (b) voltage profiles and (c) specific capacity values for a V_2O_5 IO lithium battery (i.e. vs. Li metal) over 50 cycles. (d) Schematic representation of a two electrode Li-ion cell consisting of a V_2O_5 IO cathode and a prelithiated Co_3O_4 IO anode. (e) SEM image, (f) voltage profiles and (g) specific capacity variation over 50 cycles for the Co_3O_4 IO anode cycled against a Li counter electrode. Both IO electrodes are formed directly on current collectors without conductive additives or polymeric binders.

The voltage profiles for a Co_3O_4 IO anode half-cell are shown in Figure 1f and the specific capacity values obtained over 50 cycles are shown in Figure 1g. The initial charge and discharge capacities were 1684 and 1080 mAh g^{-1}, respectively, indicating a coulombic efficiency of ~ 64%. This loss in capacity may have resulted from the formation of a solid electrolyte interface (SEI) layer due to electrolyte decomposition. However, after the first 10 cycles the decay in specific capacity values was less severe and the anode maintains an impressive 300 mAh g^{-1} after 50 cycles, making the Co_3O_4 IO a suitable anode for most cathodes in terms of capacity matching. The specific capacity values presented in Figure 1g are comparable [60-62] to and/or higher than [53, 63, 64] reported capacity values for other Co_3O_4 nanostructured electrodes. It has been previously reported that capacity fading for Co_3O_4 electrodes may be due to a decomposition of the electrolyte with increased cycling, leading to a suppression of the reaction between Li-ions and electrons at the electrode/electrolyte interface. Kang et al. performed electrochemical impedance spectroscopy after each anodic charge for 100 cycles and reported an increase in charge transfer resistance with increased cycling. [63] Co_3O_4 nanoparticles are formed instead of an inverse opal when Co_3O_4 samples are prepared without a PS sphere template coating on the stainless steel substrate, as shown in the SEM image in Figure S5a. A comparison of the specific capacity values obtained from the Co_3O_4 nanoparticles and from an IO sample in Figure S5b indicates the benefit of an IO structure, as higher specific capacity values and increased capacity retention were observed for the IO sample compared to the Co_3O_4 nanoparticles.

From the electrochemical characterization presented in Figure 1, we have demonstrated that the Co_3O_4 IO structure is a promising anode material. If there are to be significant advancements in obtainable specific capacities and cycle life stability then promising non-traditionally used cathode/anode pairings must be investigated. To transition from the conventional electrode pairings, we developed a full lithium-ion cell consisting of a V_2O_5 IO cathode and a pre-charged Co_3O_4 IO anode. The anode was electrochemically pre-charged (see Experimental, Supporting Information), ensuring that the conversion reactions at Co_3O_4 provided sufficient Li as the source for highly efficient reversibility, as will be shown. A schematic representation of our full inverted opal Li-ion cell is shown in Figure 1d. To our knowledge, this is the first report of this pairing of electrode materials as well as the first full all-oxide and inverse opal Li-ion battery.

The electrochemical characterization of our full inverse opal Li-ion battery is presented in Figure 2. The OCV for the V_2O_5 IO lithium battery was ~ 3.6 V (vs Li/Li^+), whereas for the full V_2O_5 IO/Co_3O_4 IO cell the OCV was ~ 2.6 V, approximately 1 V lower. As discussed, the Co_3O_4 IO is initially electrochemically lithiated. As can be seen in the charge curve in Figure 1f, there is a significant plateau at ~ 1 V. We propose that when the pre-lithiated Co_3O_4 IO anode is put into a clean split cell against the V_2O_5 IO cathode, the OCV of the anode relaxes back to the plateau voltage of ~ 1 V (vs Li/Li^+).

The V_2O_5 IO structure in a half cell arrangement was cycled in a potential window ranging from 4.0 – 1.2 V (vs Li/Li^+). Due to the OCV decreasing by ~1 V in the full IO cell, the effective potential window was 3.0 – 0.2 V. Commercial Li-ion batteries are typically 2-electrode cells containing a $LiCoO_2$ cathode and a graphite anode. They are typically cycled in a potential window from 4.2 – 3.0 V and have a nominal voltage of 3.7 V.

As the reference and counter electrodes are coupled together in a 2-electrode arrangement, the reference electrode is the pre-charged Co_3O_4 IO. There is no Li metal reference electrode, so the potentials described for a 2-electrode arrangement are not vs Li/Li^+, they are instead the potential difference between a V_2O_5 IO cathode and a pre-charged Co_3O_4 IO anode. It is worth noting here that if a full IO cell is prepared in a 3 electrode cell with a dedicated Li metal

reference electrode the OCV and the potential window used are the same as for when the V_2O_5 IO is tested in a half cell arrangement, which is discussed in further detail later.

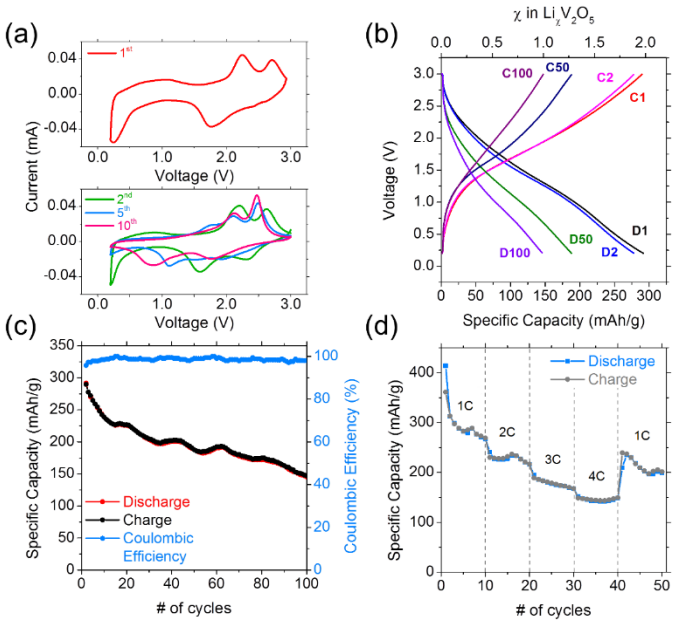

Fig. 2. Electrochemical characterization of the V_2O_5 IO/Co_3O_4 IO full Li-ion cells. (a) Cyclic voltammetry and (b) discharge and charge voltage profiles of the V_2O_5/Co_3O_4 IO battery in a 2-electrode split cell at 2.5 C rate. (c) Specific capacity values obtained during the first 100 cycles and (d) specific capacities retention obtained from variable discharge-charge rate testing. All tests were performed in 2-electrode stainless steel split cells, and the cycling is always to full depth of discharge and state of charge in each case.

Cyclic voltammetry was used initially to characterize the V_2O_5 IO/Co_3O_4 IO full cell. The cells were cycled 10 times at a scan rate of 0.1 mVs^{-1} in a potential window of 3.0 – 0.2 V. In terms of our V_2O_5 IO/Co_3O_4 IO full cell, both insertion and removal processes occur simultaneously; during discharge, the V_2O_5 IO is lithiated and the Co_3O_4 IO is recharged via more complex conversion-mode processes (see Supporting Information for details), and *vice versa* during charging. The resulting CV curves are a convolution of both electrode processes that occur simultaneously and consequently it is difficult to assign the resulting peaks observed in the voltammograms to a specific process involving the insertion/removal of Li^+ for either one of the electrode materials. The peak observed in the negative scan of the first cycle at ~ 1.77 V, shifts to ~ 1.58 V in the 2nd cycle and by the 10th cycle, the peak has decreased further in potential to ~ 0.87 V. In contrast to this the potentials of the two main peaks observed in the positive scan (between 2.0 and 3.0 V) show little variation with increased cycling.

The specific capacity and cycle life stability of the V_2O_5 IO/Co_3O_4 IO full cell was investigated through galvanostatic testing at C-rate of 2.5 C, where 1C = 147 mAh g^{-1} ($Li_\chi V_2O_5$, χ = 1). The resulting discharge/charge profiles, as presented in Figure 2b, show smooth curves without any obvious plateaus. Similar smooth curves have been observed for other nanostructured V_2O_5 electrodes. [15, 65, 66] The initial discharge response in Figure 2b confirms ~ 2 mol of Li per V_2O_5 unit in the IO cathode, in good agreement with Eqn. S2. compared to the V_2O_5 half-cell, the slightly reduced intercalated mole fraction to $Li_\chi V_2O_5$, χ = 2 is due to the lower voltage limits (3.0 – 0.2 V). After the initial charging of the Co_3O_4 anode and prior to full cell assembly, Co and Li_2O are formed. Upon discharge, these products are oxidized by the removal of an equivalent of ~2 mol of Li, which confirms an efficient reversible (de)lithiation-reversible conversion processes in the all-oxide IO cell.

The specific capacity values over 100 cycles are shown in Figure 2c. The initial discharge capacity was ~ 290 mAh g^{-1}, which is close to the theoretical specific capacity of V_2O_5 of 294 mAh g^{-1} (for $Li_\chi V_2O_5$, χ = 2). After 50 cycles the specific capacity values were ~ 190 mAh g^{-1} and after 100 cycles the capacity values maintain ~150 mAh g^{-1}. These specific capacity values would be significant for a V_2O_5 electrode cycled in a half cell versus a pure Li counter electrode. Here, they are efficiently achieved with a full Li-ion battery using pre-charged Co_3O_4 IO paired with a V_2O_5 IO cathode.

Rate capability is one of the key issues with the current generation of lithium ion batteries. In order to investigate the rate capability of the V_2O_5 IO/Co_3O_4 IO full cells, they were cycled at various C-rates ranging from 1C – 4C, where 1C = 147 mAh g^{-1} ($Li_\chi V_2O_5$, χ = 1), as shown in Figure 2d. The capacities over the first 10 cycles were ~300 mAh g^{-1}. At the highest C-rate used (4C) the specific capacity value of ~150 mAh g^{-1} was maintained. However, after 40 cycles, at the initial C-rate of 1C, the specific capacity recovered to ~230 mAh g^{-1}. Hence the full V_2O_5 IO/Co_3O_4 IO cell demonstrates significant reversible capacity, considerable capacity retention and outstanding rate performance.

The full V_2O_5 IO/Co_3O_4 IO cell is cycled from 3.0 – 0.2 V, a lower potential window than the most commonly used Li-ion cell electrode pairing. For practical use, several V_2O_5 IO/Co_3O_4 IO cells could be connected in series to raise the nominal voltage, depending on the power requirement. The nominal voltage for both NiCd and NiMH batteries is 1.2 V. In both cases three cells are usually connected in series to boost the nominal voltage to 3.6 V, which is comparable to the 3.7 V nominal voltage of standard Li-ion batteries. We propose that for practical use in consumer electronics, three V_2O_5 IO/Co_3O_4 IO cells could be connected in series to power devices which require a nominal operating voltage of ~ 3.7 V, while maintaining high capacity and rate-stable cycle life.

Asymmetric discharging and charging is one practical battery testing technique that is often overlooked. This technique enables slow discharging and fast charging of cells. This ultimately represents what consumers demand from their electronic devices that are powered by Li-ion batteries, i.e. to charge the device quickly and discharge the device slowly with full power. To investigate the practical application of our V_2O_5 IO/Co_3O_4 IO full cell, asymmetric cycling was performed using a constant current of 25 μA during discharging and 100 μA during charging, these current values corresponded to C-rates of 2 C and 8 C, respectively, where 1C = 147 mAh g^{-1} ($Li_\chi V_2O_5$, χ = 1). The discharge time for current generation smartphones is on average four to five times the charge time, hence we desired to test the full V_2O_5 IO/Co_3O_4 IO cell with a similar

asymmetry. The results of the asymmetric testing of the full inverse opal cells are presented in Figure 3.

The first 5 cycles in Figure 3a, demonstrate the time difference in discharge and charge segments due to the asymmetric C-rates which were used for each process. The discharge and charge voltage profiles shown in Figure 3b are quite similar to the voltage profiles shown in Figure 2b but the initial discharge capacity for the asymmetric testing of the all-IO cell was higher. After 60 cycles the discharge capacity for both cells was approximately the same at ~ 190 mAh g^{-1}. The increased capacity is also reflected in the intercalated Li mole fraction of the $Li_xV_2O_5$ IO cathode. Initially ~ 2.7 mol of Li were inserted into the V_2O_5 IO for the asymmetric test compared to the ~ 2.0 mol inserted initially during the galvanostatic test presented in Figure 2. The increased first cycle capacity is obtained at a slightly lower discharge current, and reflected in a slightly higher Li mole fraction for the cathode. Any capacity from irreversible decomposition of the electrolyte [63] is discussed further in a later section.

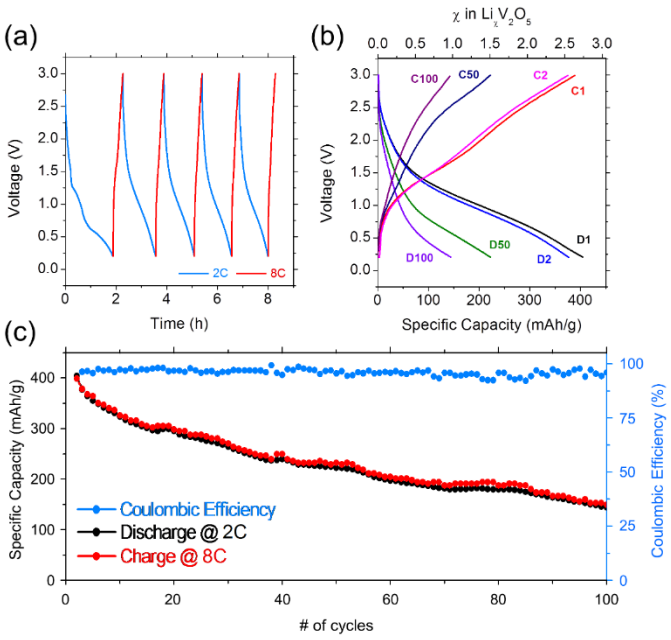

Fig. 3. Asymmetric charge-discharge profiling of a V_2O_5 IO/Co_3O_4 IO full Li-ion cell. (a) Asymmetric discharge (2 C-rate) and charge (8 C-rate) over the first 5 cycles. The voltage profiles remain consistent even with a fast charge of the cathode/discharge of the anode in successive cycles. (b) Discharge and charge voltage profiles selected from 100 cycles and (c) specific capacity values over 100 cycles with consistent coulometric efficiency during asymmetric discharge and charging. Tests were performed in a 2-electrode stainless steel split cell.

The specific capacity values over 100 cycles and the corresponding coulombic efficiencies are shown in Figure 3c. The initial capacities of ~ 400 mAh g^{-1} decreased quickly over the first 20 cycles, after which the discharge capacity had decreased to ~ 295 mAh g^{-1}. However from the 20th to the 100th there is a more gradual fading of capacity values. After 100 cycles the specific capacity remained stable at ~145 mAh g^{-1}, which is a significant capacity to achieve from a full Li-ion battery after 100 cycles. By cycling the full IO cell asymmetrically it may be expected that the charge capacities would be significantly lower than the discharge capacities due to the difference in the C-rates used for discharging and charging. Interestingly however, this is not the case for the V_2O_5 IO/Co_3O_4 IO full cell, as can be seen in Figure 3c. We note excellent correlation between the discharge and charge capacities over 100 cycles, and maintained in consistent Coulombic efficiencies >98%. During asymmetric testing the full V_2O_5 IO/Co_3O_4 IO cell consistently delivered specific capacity values >150 mAh g^{-1} for 100 cycles. This is a significant finding and demonstrates that the full V_2O_5 IO/Co_3O_4 IO cell can be charged quickly and discharged slowly without rapid capacity decay. The V_2O_5 IO/Co_3O_4 IO full cell is a promising full Li-ion cell architecture for use in consumer electronics typically powered by Li-ion batteries, providing good, stable capacities at different rates of charge and discharge.

As mentioned earlier, all of the electrochemical tests presented above were performed in 2-electrode split cells using a glass fibre separator soaked in electrolyte. In order to determine if there is a contribution to the initial specific capacity values due to the decomposition of the electrolyte [67], V_2O_5 IO/Co_3O_4 IO full cells were cycled galvanostatically in a flooded cell arrangement, whereby the electrolyte was in excess and the impact of any such breakdown of the electrolyte would be negligible compared to the electrolyte volume. Many complex 3D material architectures, whether ordered or randomly networked, can cause variations in local electric field and ionic concentration gradients towards and within the materials, in spite of their nominal benefits of interconnectedness and reduced ionic diffusion distances. Non-uniform ionic gradients and diffusion lengths are exacerbated by limited electrolyte and non-uniform soakage of all the porous architecture. Locally high current densities in certain regions can promote different rates of lithiation, and perhaps irreversible phases for some materials, and thus we adopted a flooded electrode arrangement to unequivocally address this issue, with and without a fresh Li reference. Additionally, the standard forms of electrolyte soaked separator, whether porous polypropylene or glass fiber, cannot formally ensure electrolyte wetting of 3D structured nanocrystalline materials even under compression. Electrochemical tests in flooded cells were performed in a 2-electrode arrangement to allow direct comparison with results obtained in 2-electrode split cells, and also in a 3-electrode arrangement with a Li reference electrode. The Li mole fraction for the discharged V_2O_5 IO is ~1.0 mol (Figure 4a) in the electrolyte flooded 2-electrode cell, which is approximately half that observed in a split cell (Figure 2b). This variation in calculated Li mole fraction may be due to decomposition of the electrolyte in the split cell configuration.

It has previously been reported that decomposition of the electrolyte may result in a higher initial capacity[68] and consequently a higher calculated Li mole fraction. The initial value after the first discharge of ~0.90 mol increased slightly to ~1.03 mol after 100 cycles in the flooded cell, a significant improvement over the cells cycled in split cells, which decreased from ~2 to ~1 mol of Li inserted over 100 cycles, in line with capacity. The consistent reversibility and intercalated

phase confirms that effective electrode-electrolyte wetting is critical for maintaining high capacity with stable reversibility in porous functional battery materials.

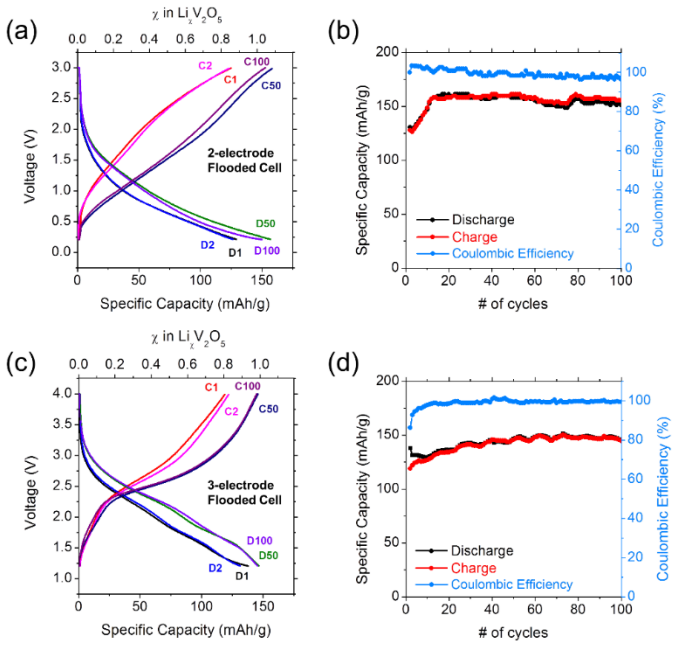

Fig. 4. Enhancing cycle life in full-IO batteries using efficient electrolyte wetting. (a) Discharge and charge voltage profiles and (b) specific capacity values over the first 100 cycles for a V_2O_5 IO/Co_3O_4 IO full cell cycled in a 2-electrode flooded cell. (c) Discharge and charge voltage profiles and (d) specific capacity values over the first 100 cycles for a V_2O_5 IO/Co_3O_4 IO full cell cycled in a 3-electrode flooded cell with a Li reference electrode.

The specific capacity values for a full IO cell cycled in a 2-electrode flooded cell over 100 cycles are shown in Figure 4b. The capacity values increased over the first 15 cycles from ~130 to ~160 mAh g^{-1}, and notably, is as high as the half-cell but never degrades with cycling. This observation is unique in this case, to the full IO cell, where the Li source is from the pre-charged Li_2O phase at the Co_3O_4 IO anode. From the 15th to the 100th cycle the full IO cell displays excellent stability in terms of capacity retention, with an average discharge capacity of ~156 mAh g^{-1}. Stable capacity retention for a large number of cycles is crucial for commercial Li-ion batteries; here we demonstrate significant stable capacity values over the first 100 cycles for a full inverse opal structured Li-ion cell containing a non-traditional cathode/anode electrode pairing.

When full Li-ion cells are cycled in a 2-electrode configuration, the reference electrode is typically connected to the counter electrode (anode). As explained by Eqn. S1-S3, the Co_3O_4 IO anode used in these full IO cells is a conversion material, which cycles by the reversible formation and decomposition of Li_2O and Co_3O_4 reduction and oxidation. The Li metal reference electrode allows unambiguous assessment of voltage profiles for all IO cell types, and remains unaltered during cycling. Hence, we also cycled the V_2O_5 IO/Co_3O_4 IO full cells in a 3-electrode flooded cell with Li metal reference electrode and the data is shown in Figure 4c and d. The cell's initial OCV was ~3.6 V (vs Li/Li^+), which is ~1 V higher than the full IO cell in a 2-electrode arrangement, but similar to the OCV of the V_2O_5 IO lithium battery. Consequently, the 3-electrode cell full V_2O_5 IO/Co_3O_4 IO cell was cycled from 4.0 – 1.2 V (vs Li/Li^+).

The discharge and charge profiles for the 1st, 2nd, 50th and 100th cycles are shown in Figure 4c. The Li mole fractions in the discharged V_2O_5 IO structure in a 3-electrode flooded cell after the 1st and 100th discharged were ~0.94 and ~0.99 mol, respectively. These values are almost identical to the 2-electrode flooded cell (Figure 4a). However, there are differences in shape of the voltage profiles for 2 and 3-electrode flooded cell discharging-charging. In the 2-electrode flooded cell the discharge and charge curves are smooth and without any obvious stable voltage plateau. In the 3-electrode flooded cell with a Li reference electrode, voltage variations in IO cathodes were observed in the discharge curves at ~1.56 and ~2.08 V, which correspond to ε-$Li_\chi V_2O_5$ and δ-$Li_\chi V_2O_5$ phase transitions. [69] In both 2-electrode and Li-referenced 3-electrode flooded cells, we find that capacity retention is excellent and is found to increase over 100 cycles, without any adverse changes to the electrochemical response or voltage profiles.

The specific capacity values for the full IO cell tested in a 3 electrode flooded cell are shown in Figure 4d. The initial capacities (~138 mAh g^{-1}) were quite similar to the values obtained in a 2-electrode flooded cell, and excellent specific capacity stability over 100 cycles is possible, with an average discharge capacity of ~144 mAh g^{-1}, demonstrating that the V_2O_5 IO/Co_3O_4 IO full cell can deliver stable capacity retention over a large number of cycles. There is a clear correlation between the performance of cells cycled in 2 and 3 electrode flooded cells in terms of the number of moles of lithium inserted and the specific capacity values. The fine detail, such as observable features in V_2O_5 discharge voltage profiles, is convoluted with the corresponding Co_3O_4 charge voltage profiles for the 2-electrode flooded cell measurements, in the absence of a Li reference electrode. The Li reference electrode in full Li-ion cells provides insight into processes that are obscured by using the anode as both the counter and reference electrodes. This could lead to a greater understanding of capacity fading issues in full cells that use non-traditional or new pairings of the many high performance materials reported as lithium batteries (cathodes) or half-cells (anodes).

Finally, a comparison of the discharge capacities obtained for our V_2O_5 IO/Co_3O_4 IO full cells cycled in a 2-electrode split cell, a 2 electrode flooded cell and also a 3 electrode flooded cell with a Li reference electrode, is presented in Figure 5a. The initial capacities in the 2-electrode split cell were significantly higher than the initial capacities obtained in both 2 and 3-electrode flooded cells. The higher capacity observed during the initial cycles is not observed when the porous material is efficiently wetted with electrolyte. Most importantly, in flooded IO batteries, a stable capacity is maintained with no initial capacity loss nor any fading during cycling in both symmetric and asymmetric charge-discharge conditions. The similarity of the 2- and 3-electrode flooded cells confirms that lithium reactivity changes do not adversely affect capacity or cycle life provided the cell maintains electrolyte supply to all

active material. Decomposition of the electrolyte results in higher initial capacities however it also results in significant capacity fading after a large number of cycles. [68] After the 175th discharge the specific capacity for the full IO cell tested in a split cell was ~63 mAh g^{-1}, corresponding to a ~78 % loss in the initial capacity.

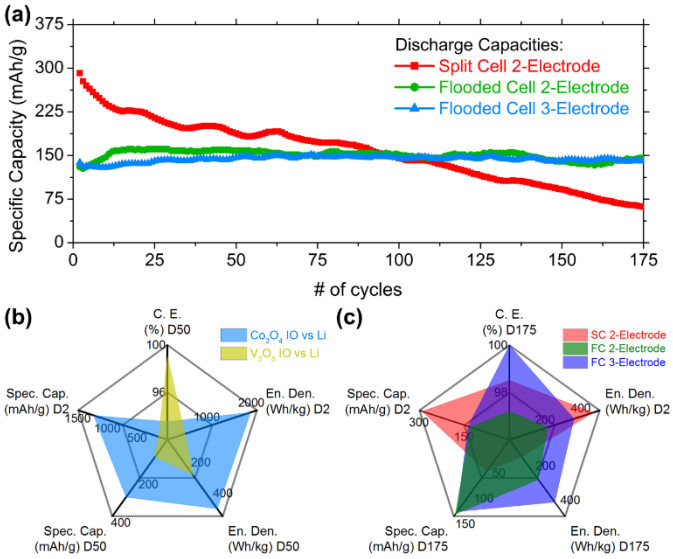

Fig. 5. Stable capacity retention in V_2O_5 IO/Co_3O_4 IO full cells. (a) A comparison of the discharge capacities obtained for V_2O_5 IO/Co_3O_4 IO full cells cycled in a 2-electrode split cell and 2 and 3-electrode flooded cells. Radar plots comparing the coulombic efficiency, energy density and specific capacity values for (b) V_2O_5 IO cathodes and Co_3O_4 IO anodes in lithium half cells and (c) V_2O_5 IO/Co_3O_4 IO full cells cycled in a 2-electrode split cell and 2 and 3-electrode flooded cells. D2, D50 and D175 refer to the 2nd, 50th and 175th discharge. Legend: En. Den. = energy density, C. E. = coulometric efficiency, Spec. Cap. = specific capacity.

V_2O_5 IO/Co_3O_4 IO full cells, cycled in flooded cells, demonstrated outstanding capacity stability over 175 cycles. The average specific capacity values for the 2 and 3-electrode flooded cells over 175 cycles were ~150 and ~144 mAh g^{-1} respectively. While the average specific capacity was slightly higher in the 2-electrode flooded cell, the standard deviation was lower in the 3-electrode flooded cell. The standard deviation in the capacity values for the 2 and 3-electrode flooded cells were ~7.8 and ~4.8 mAh g^{-1} respectively, and are postulated to benefit from better electrolyte wetting of all the IO active nanocrystalline material in both electrodes. The stable specific capacity values of ~150 mAh g^{-1} obtained for the V_2O_5

IO/Co_3O_4 IO full cell over 175 cycles are higher than capacity values reported for several different full Li-ion cell electrode pairings including a $LiCoO_2/Li_4Ti_5O_{12}$ electrode pairing (~120 mAh g^{-1}) [70, 71], a $LiMn_2O_4/Li_4Ti_5O_{12}$ electrode pairing (~100 mAh g^{-1}) [72], a $LiFePO_4/Li_4Ti_5O_{12}$ electrode pairing (~120 mAh g^{-1}) and a $LiCoO_2$/lithium-polymer silicon electrode pairing (~125 mAh g^{-1}). [73] It is clear from Figure 5a that the V_2O_5 IO/Co_3O_4 IO full cell is significantly improved from having an excess of electrolyte within the active material and the cell that effectively mitigates the impact and contribution of electrolyte breakdown at the nanocrystalline surfaces of the IOs. The findings also demonstrate that electrolyte effects and the dual-mode operation of the cathode and anode pair contribute to higher initial capacities, and electrolyte effects seem to influence capacity fading during long term cycling predominantly. The level of capacity stability observed for the full IO cell in a flooded cell arrangement represents the level of performance that is desirable in commercial Li-ion batteries, i.e. a consistently stable capacity over a large number of cycles as opposed to a Li-ion battery whose capacity steadily fades with increased cycling and charge rate.

Conclusions

The development of an all oxide, all inverse opal Li-ion battery that demonstrates excellent capacity, cycle life, and performance is possible using 3D structured materials. While V_2O_5 and Co_3O_4 IO structures are promising cathode and anode materials in their own right, the first successful pairing of intercalation mode cathode and conversion-mode anode demonstrates that overall cell performance is enhanced in a voltage range where the electrochemical response of both electrodes contributes to stable capacity retention. By effective pre-charging of the Co_3O_4 IO anode via conversion mode formation of Li_2O and Co, the efficiency of reversible lithium intercalation is improved by limiting it to the cathode potential window. The anode also avoids the need for a stable SEI formation. The novel V_2O_5/Co_3O_4 pairing reported here is a paradigm shift towards embracing non-traditionally used electrode materials in electrode pairings, while benefitting from different charge storage mechanisms that together show superior response compared to their respective half-cells and lithium batteries.

In 2-electrode V_2O_5 IO/Co_3O_4 IO Li-ion cells, capacities > 150 mAh g^{-1} were retained after 100 cycles, which is higher than the capacities reported for many full Li-ion cells. Rate capability tests of the full IO cell demonstrated significant reversible capacity of ~ 200 mAh g^{-1}, considerable capacity retention after 50 cycles and outstanding rate performance. Through asymmetric testing, we have shown that the V_2O_5 IO/Co_3O_4 IO full Li-ion cell can be charged quickly (8C) and discharged relatively slowly (2C – which is still quite fast for some applications) without rapid capacity fade. The reversible formation and decomposition of Li_2O during charging and discharging of the Co_3O_4 IO electrode that contributes to charge in the initial cycles from electrolyte decomposition is a function of the available electrolyte volume. With the benefits of nanoscale materials and 3D structure demonstrated in both the anode and cathode, the need for effective infiltration of electrolyte in nanoscale and porous materials was shown to be critical in maintaining high capacity and its retention over many cycles. For conversion mode anodes and effective intercalation in 3D structured or porous cathodes, electrolyte soaking ensures constant Li-ion concentration and solubilisation (without build up) of Li_2O. Full IO cells using dual-mode oxide pairs showed no initial capacity loss or any capacity fade over 175 cycles, while maintaining a high capacity, a stable overall cell voltage and energy density. The successful pairing of two electrode materials in inverse opal structure, without binders or conductive additives, operating under distinctly different charge storage modes, augers well

for development of non-traditional material pairs for Li-ion and emerging alternative batteries and for fast charge/discharge rate stable operation with high, stable capacity and energy densities.

Acknowledgements

This work was supported by an Science Foundation Ireland Technology Innovation and Development Award under contract no. 13/TIDA/E2761. This research has received funding from the Seventh Framework Programme FP7/2007-2013 (Project STABLE) under grant agreement no. 314508. We also acknowledge the support of the Irish Research Council under award RS/2010/2920 and a New Foundations Award. This publication has also emanated from research supported in part by a research grant from SFI under Grant Number 14/IA/2581.

Notes and references

1. J. Cabana, L. Monconduit, D. Larcher and M. R. Palacin, *Advanced Materials*, 2010, **22**, E170-E192.
2. V. Etacheri, R. Marom, R. Elazari, G. Salitra and D. Aurbach, *Energy & Environmental Science*, 2011, **4**, 3243-3262.
3. J. B. Goodenough and K.-S. Park, *Journal of the American Chemical Society*, 2013, **135**, 1167-1176.
4. M. M. Thackeray, C. Wolverton and E. D. Isaacs, *Energy & Environmental Science*, 2012, **5**, 7854-7863.
5. H. Wang, Y. Yang, Y. Liang, J. T. Robinson, Y. Li, A. Jackson, Y. Cui and H. Dai, *Nano Letters*, 2011, **11**, 2644-2647.
6. P. G. Bruce, S. A. Freunberger, L. J. Hardwick and J.-M. Tarascon, *Nature materials*, 2012, **11**, 19-29.
7. M. D. Bhatt, H. Geaney, M. Nolan and C. O'Dwyer, *Physical Chemistry Chemical Physics*, 2014, **16**, 12093-12130.
8. M. M. Thackeray, S.-H. Kang, C. S. Johnson, J. T. Vaughey, R. Benedek and S. Hackney, *Journal of Materials Chemistry*, 2007, **17**, 3112-3125.
9. K. Shaju, G. S. Rao and B. Chowdari, *Electrochimica Acta*, 2002, **48**, 145-151.
10. F. Lin, I. M. Markus, D. Nordlund, T.-C. Weng, M. D. Asta, H. L. Xin and M. M. Doeff, *Nature Communications*, 2014, **5**, 3529.
11. Z. Xie, H. Eikhuemelo, J. Zhao, C. Cain, W. Xu and Y. Wang, *Journal of The Electrochemical Society*, 2015, **162**, A1523-A1529.
12. S. Liu, J. Wu, J. Zhou, G. Fang and S. Liang, *Electrochimica Acta*, 2015, **176**, 1-9.
13. L.-H. Hu, F.-Y. Wu, C.-T. Lin, A. N. Khlobystov and L.-J. Li, *Nature communications*, 2013, **4**, 1687.
14. Y. Zhao, L. Peng, B. Liu and G. Yu, *Nano Letters*, 2014, **14**, 2849-2853.
15. D. McNulty, D. Buckley and C. O'Dwyer, *Journal of The Electrochemical Society*, 2014, **161**, A1321-A1329.
16. Q. Liu, Z.-F. Li, Y. Liu, H. Zhang, Y. Ren, C.-J. Sun, W. Lu, Y. Zhou, L. Stanciu and E. A. Stach, *Nature communications*, 2015, **6**, 6127.
17. J. Wang, C. Cui, G. Gao, X. Zhou, J. Wu, H. Yang, Q. Li and G. Wu, *RSC Advances*, 2015, **5**, 47522-47528.
18. C. de las Casas and W. Li, *Journal of Power Sources*, 2012, **208**, 74-85.
19. J. Zhang, Z. Xie, W. Li, S. Dong and M. Qu, *Carbon*, 2014, **74**, 153-162.
20. G. Kucinskis, G. Bajars and J. Kleperis, *Journal of Power Sources*, 2013, **240**, 66-79.
21. V. Etacheri, C. N. Hong and V. Pol, *Environmental Science and Technology*, 2015, **49**, 11191–11198.
22. C. K. Chan, H. Peng, G. Liu, K. McIlwrath, X. F. Zhang, R. A. Huggins and Y. Cui, *Nature Nanotechnology*, 2008, **3**, 31-35.
23. P. Nithyadharseni, M. Reddy, B. Nalini, M. Kalpana and B. Chowdari, *Electrochimica Acta*, 2015, **161**, 261-268.
24. T. Kennedy, E. Mullane, H. Geaney, M. Osiak, C. O'Dwyer and K. M. Ryan, *Nano Letters*, 2014, **14**, 716–723.
25. J. Liu, H. G. Zhang, J. Wang, J. Cho, J. H. Pikul, E. S. Epstein, X. Huang, J. Liu, W. P. King and P. V. Braun, *Advanced Materials*, 2014, **26**, 7096-7101.
26. R. Verrelli and J. Hassoun, *ChemElectroChem*, 2015, **2**, 988–994.
27. L. Zhang, H. B. Wu and X. W. D. Lou, *Advanced Energy Materials*, 2014, **4**.
28. R. Malini, U. Uma, T. Sheela, M. Ganesan and N. Renganathan, *Ionics*, 2009, **15**, 301-307.
29. N. Nitta, F. Wu, J. T. Lee and G. Yushin, *Materials today*, 2015, **18**, 252-264.
30. P. G. Bruce, B. Scrosati and J. M. Tarascon, *Angewandte Chemie International Edition*, 2008, **47**, 2930-2946.
31. C. P. Rhodes, J. W. Long, K. A. Pettigrew, R. M. Stroud and D. R. Rolison, *Nanoscale*, 2011, **3**, 1731-1740.
32. J. W. Long, B. Dunn, D. R. Rolison and H. S. White, *Chemical Reviews*, 2004, **104**, 4463-4492.
33. J. H. Pikul, H. Gang Zhang, J. Cho, P. V. Braun and W. P. King, *Nature Communications*, 2013, **4**, 1732.
34. E. Armstrong, D. McNulty, H. Geaney and C. O'Dwyer, *ACS Appl. Mater. Interfaces*, 2015, **7**, 27006-27015.
35. E. Armstrong and C. O'Dwyer, *Journal of Materials Chemistry C*, 2015, **3**, 6109-6143.
36. A. Vu and A. Stein, *Chemistry of Materials*, 2011, **23**, 3237-3245.
37. D.-Y. Kang, S.-O. Kim, Y. J. Chae, J. K. Lee and J. H. Moon, *Langmuir*, 2013, **29**, 1192-1198.
38. C. O'Dwyer, *Adv. Mater.*, 2016, DOI: 10.1002/adma.201503973.
39. A. Vu, Y. Qian and A. Stein, *Advanced Energy Materials*, 2012, **2**, 1056-1085.
40. A. Stein, *Nature Nanotechnology*, 2011, **6**, 262-263.
41. H. Zhang, X. Yu and P. V. Braun, *Nature Nanotechnology*, 2011, **6**, 277-281.
42. N. D. Petkovich, S. G. Rudisill, B. E. Wilson, A. Mukherjee and A. Stein, *Inorganic chemistry*, 2014, **53**, 1100-1112.
43. M. Osiak, H. Geaney, E. Armstrong and C. O'Dwyer, *Journal of Materials Chemistry A*, 2014, **2**, 9433-9460.
44. U. von Sacken, E. Nodwell, A. Sundher and J. Dahn, *Journal of Power Sources*, 1995, **54**, 240-245.
45. R. Bhattacharyya, B. Key, H. Chen, A. S. Best, A. F. Hollenkamp and C. P. Grey, *Nature materials*, 2010, **9**, 504-510.
46. P. Balakrishnan, R. Ramesh and T. P. Kumar, *Journal of Power Sources*, 2006, **155**, 401-414.

47. Q. Wang, P. Ping, X. Zhao, G. Chu, J. Sun and C. Chen, *Journal of Power Sources*, 2012, **208**, 210-224.
48. C. Liu, E. I. Gillette, X. Chen, A. J. Pearse, A. C. Kozen, M. A. Schroeder, K. E. Gregorczyk, S. B. Lee and G. W. Rubloff, *Nature Nanotechnology*, 2014, **9**, 1031-1039.
49. E. Armstrong, M. Osiak, H. Geaney, C. Glynn and C. O'Dwyer, *CrystEngComm*, 2014, **16**, 10804-10815.
50. E. Armstrong, M. O'Sullivan, J. O'Connell, J. D. Holmes and C. O'Dwyer, *J. Electrochem. Soc.*, 2015, **162**, D605-D612.
51. M. Okubo, E. Hosono, T. Kudo, H. S. Zhou and I. Honma, *Solid State Ionics*, 2009, **180**, 612-615.
52. S. Lim, C. S. Yoon and J. Cho, *Chemistry of Materials*, 2008, **20**, 4560-4564.
53. K. M. Shaju and P. G. Bruce, *Chemistry of Materials*, 2008, **20**, 5557-5562.
54. H. g. Wang, D. l. Ma, Y. Huang and X. b. Zhang, *Chemistry-A European Journal*, 2012, **18**, 8987-8993.
55. H. X. Li, L. F. Jiao, H. T. Yuan, M. Zhang, J. Guo, L. Q. Wang, M. Zhao and Y. M. Wang, *Electrochemistry Communications*, 2006, **8**, 1693-1698.
56. V. M. Mohan, B. Hu, W. Qiu and W. Chen, *J Appl Electrochem*, 2009, **39**, 2001-2006.
57. A. I. Popa, E. Vavilova, C. Täschner, V. Kataev, B. Büchner and R. Klingeler, *The Journal of Physical Chemistry C*, 2011, **115**, 5265-5270.
58. X. Zhou, G. Wu, G. Gao, J. Wang, H. Yang, J. Wu, J. Shen, B. Zhou and Z. Zhang, *The Journal of Physical Chemistry C*, 2012, **116**, 21685-21692.
59. X. Xia, J. Tu, J. Zhang, J. Xiang, X. Wang and X. Zhao, *ACS applied materials & interfaces*, 2009, **2**, 186-192.
60. D. Su, X. Xie, P. Munroe, S. Dou and G. Wang, *Scientific Reports*, 2014, **4**, 6519.
61. D. Gu, W. Li, F. Wang, H. Bongard, B. Spliethoff, W. Schmidt, C. Weidenthaler, Y. Xia, D. Zhao and F. Schüth, *Angewandte Chemie International Edition*, 2015.
62. X. Wang, X. Chen, L. Gao, H. Zheng, Z. Zhang and Y. Qian, *Journal of Physical Chemistry B*, 2004, **108**, 16401-16404.
63. J.-G. Kang, Y.-D. Ko, J.-G. Park and D.-W. Kim, *Nanoscale Res Lett*, 2008, **3**, 390-394.
64. G. Pan, X. Xia, F. Cao, J. Chen and Y. Zhang, *Electrochimica Acta*, 2015, **173**, 385–392.
65. D. McNulty, D. N. Buckley and C. O'Dwyer, *ECS Transactions*, 2013, **50**, 165-174.
66. K. West, B. Zachau-Christiansen, T. Jacobsen and S. Skaarup, *Electrochimica Acta*, 1993, **38**, 1215-1220.
67. D. Ruzmetov, V. P. Oleshko, P. M. Haney, H. J. Lezec, K. Karki, K. H. Baloch, A. K. Agrawal, A. V. Davydov, S. Krylyuk, Y. Liu, J. Huang, M. Tanase, J. Cumings and A. A. Talin, *Nano Letters*, 2012, **12**, 505-511.
68. Y.-M. Kang, M.-S. Song, J.-H. Kim, H.-S. Kim, M.-S. Park, J.-Y. Lee, H. K. Liu and S. X. Dou, *Electrochimica Acta*, 2005, **50**, 3667-3673.
69. C. Delmas, H. Cognac-Auradou, J. M. Cocciantelli, M. Ménétrier and J. P. Doumerc, *Solid State Ionics*, 1994, **69**, 257-264.
70. N. Singh, C. Galande, A. Miranda, A. Mathkar, W. Gao, A. L. M. Reddy, A. Vlad and P. M. Ajayan, *Scientific reports*, 2012, **2**, 481.
71. L. Hu, H. Wu, F. La Mantia, Y. Yang and Y. Cui, *ACS Nano*, 2010, **4**, 5843-5848.
72. Y. Yang, S. Jeong, L. Hu, H. Wu, S. W. Lee and Y. Cui, *Proceedings of the National Academy of Sciences*, 2011, **108**, 13013-13018.
73. A. Vlad, A. L. M. Reddy, A. Ajayan, N. Singh, J.-F. Gohy, S. Melinte and P. M. Ajayan, *Proceedings of the National Academy of Sciences*, 2012, **109**, 15168-15173.